NJC

PAPER

View Article Online
View Journal | View Issue

Cite this: *New J. Chem.*, 2014, **38**, 1503

Sensitive and selective colorimetric sensing of Fe^{3+} ion by using *p*-amino salicylic acid dithiocarbamate functionalized gold nanoparticles†

Vaibhavkumar N. Mehta,[a] Suresh Kumar Kailasa*[a] and Hui-Fen Wu[bc]

Received (in Montpellier, France) 23rd November 2013,
Accepted 7th December 2013

DOI: 10.1039/c3nj01468a

www.rsc.org/njc

We have developed a selective and sensitive colorimetric method for determination of Fe^{3+} ion by using *p*-amino salicylic acid dithiocarbamate functionalized gold nanoparticles (DTC-PAS-Au NPs) as colorimetric probes. The DTC-PAS-Au NPs were characterized by FT-IR, ^{1}H NMR, UV-visible spectrometry, transmission electron microscopy (TEM), dynamic light scattering (DLS) and atomic force microscopic (AFM) techniques, respectively. The DTC-PAS-Au NPs are aggregated rapidly by addition of Fe^{3+} ions, yielding a color change from red to blue. The characteristic surface plasmon resonance (SPR) peak (520 nm) of DTC-PAS-Au NPs was shifted to longer wavelength, 700 nm, which confirms the ligand-to-metal charge transfer between DTC-PAS-Au NPs and Fe^{3+} ions. Under the optimal conditions, a good linear relationship (correlation coefficient R^2 = 0.993) was obtained between the ratio of the extinction at 700 nm to that at 520 nm and the concentration of Fe^{3+} over the range of 40–80 μM, with a detection limit of 14.82 nM. The DTC-PAS-Au NPs acted as colorimetric sensors for the selective detection of Fe^{3+} ions in real samples (blood and urine samples).

Introduction

Development of novel colorimetric sensors has attracted significant interest for selective and sensitive detection of metal ions in environmental and biological samples.[1–5] Iron is the most abundant vital transition metal in both plants and the human body that plays a significant role in cellular metabolism, and enzymatic catalysis. It acts as a carrier for oxygen and electron transports in hemoglobin and serves as a cofactor in many enzymatic reactions.[6–10] However, excess amounts of Fe^{3+} ion can cause damage to cellular lipids, nucleic acids and proteins. Furthermore, a deficiency of Fe^{3+} ion limits oxygen delivery to cells and causes anemia, liver and kidney damage, diabetes, and heart disease.[11–13] Therefore, the detection of Fe^{3+} ions has become a matter of considerable interest in environmental and biological samples. Conventional Fe^{3+} assays are performed by using several analytical techniques such as inductively coupled-plasma atomic emission spectrometry (ICP-AES),[14] inductively coupled plasma mass spectrometry (ICPMS),[15,16] atomic absorption spectrometry (AAS)[17] and voltammetry.[18] However, these methods are expensive and require tedious sample pretreatment procedures. Therefore, the development of a facile, inexpensive, selective and *in situ* method that allows real-time monitoring of metal species is a great challenge.

In recent years, significant research efforts have been devoted to the design and preparation of Au NPs as promising colorimetric probes for the analysis of a wide variety of molecules in environmental and biological samples.[19–22] The colorimetric sensing approaches are based on their SPR spectral shift by a strong overlap between the plasmon fields of the nearby particles, and the resulting color change from red to blue.[23–25] This is due to the strong interactions between the tailored organic molecules on the Au NPs and the target analytes, which allow Au NP-induced aggregation with the analytes. Therefore, surface functionalization of Au NPs plays a crucial role in increasing their analytical applicability for detection of trace analytes with high selectivity and sensitivity.[24,26] In this connection, dithiocarbamate molecular assembly on Au NPs has attracted significant interest in the area of nanoanalytical science due to their easy preparation and the very short interatomic distance between the two sulfur atoms which facilitates a strong binding with the NP surface.[27] As a result, dithiocarbamate derivative functionalized Au NPs have been used as selective probes for detection of biomolecules,[28] anions[29] and cations.[30,31]

[a] *Department of Applied Chemistry, S. V. National Institute of Technology, Surat-395007, India. E-mail: sureshkumarchem@gmail.com, skk@ashd.svnit.ac.in; Fax: +91-261-2227334; Tel: +91-261-2201730*

[b] *Department of Chemistry and Center for Nanoscience and Nanotechnology, Institute of Medical Science and Technology, Doctoral Degree Program in Marine Biotechnology, National Sun Yat-Sen University, Kaohsiung, 804, Taiwan*

[c] *School of Pharmacy, College of Pharmacy, Kaohsiung Medical University, Kaohsiung, 806, Taiwan*

† Electronic supplementary information (ESI) available. See DOI: 10.1039/c3nj01468a

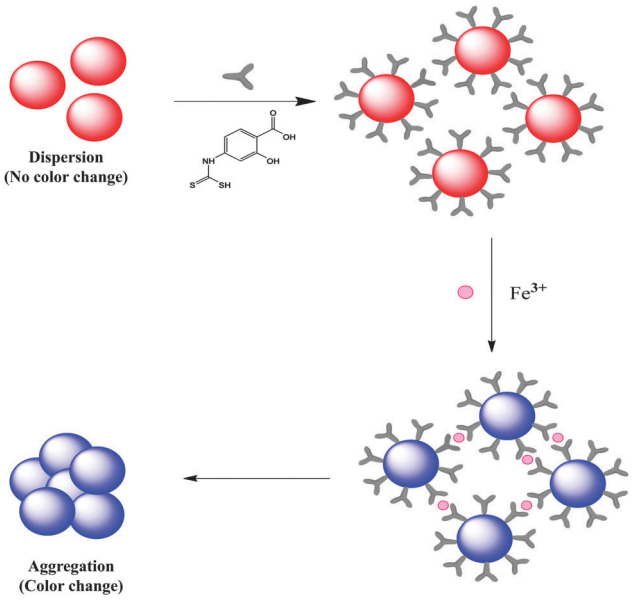

Scheme 1 Schematic representation for colorimetric sensing of Fe^{3+} by using DTC-PAS-Au NPs as colorimetric probes.

In this paper, we explore the utility of DTC-PAS-Au NPs as a colorimetric probe for the detection of Fe^{3+} in environmental and biological samples. The DTC-PAS-Au NPs aggregated rapidly by addition of Fe^{3+} ions, resulting in a color change from red to blue, which is induced by ligand-to-metal charge transfer between the –OH and –COOH groups of DTC-PAS-Au NPs and Fe^{3+} (Scheme 1). This colorimetric probe opens up new possibilities for developing analytical methods for the monitoring of Fe^{3+} in biological samples without any sample pretreatment procedure.

Experimental

Chemicals and materials

Hydrogen tetrachloroaurate hydrate ($HAuCl_4{\cdot}xH_2O$), *p*-amino salicylic acid, metal salts ($Zn(NO_3)_2{\cdot}6H_2O$, $Mn(NO_3)_2{\cdot}4H_2O$, $Co(NO_3)_2{\cdot}6H_2O$, $Pb(NO_3)_2$, $Cd(NO_3)_2{\cdot}4H_2O$, $Cu(NO_3)_2{\cdot}3H_2O$, $Hg(NO_3)_2{\cdot}H_2O$, $FeCl_2{\cdot}4H_2O$, $Mg(NO_3)_2{\cdot}6H_2O$, $NiSO_4{\cdot}6H_2O$, $FeCl_3{\cdot}6H_2O$), phosphate-buffered saline (PBS), Tris-HCl (Tris) and sodium acetate (NaAc) were obtained from Sigma-Aldrich, USA. Dimethyl formaldehyde (DMF) and carbon disulfide were purchased from Merck Ltd., India. Trisodium citrate dihydrate was purchased from SD Fine Chemicals Ltd., India. Blood and urine samples were collected from healthy volunteers. All chemicals were of analytical grade and used without further purification. Milli-Q-purified water was used for the sample preparations. **Caution**: blood samples were obtained from Shivam Pathological Laboratory, Surat, Gujarat, India, which is approved by All India Institute of Medical Sciences, New Delhi, India. The blood samples were collected by confirming informed consent. All experiments were performed in compliance with the relevant laws and institutional guidelines, and this study was also approved by the Institute Research Committee, S. V. National Institute of Technology, Surat, Gujarat, India.

Synthesis of DTC-PAS-Au NPs

Dithiocarbamate derivative of *p*-amino salicylic acid was synthesized according to the method reported in the literature.[32] Briefly, an equimolar mixture of *p*-amino salicylic acid and CS_2 in ethanolic KOH (50 mL, 5%) and DMF (50 mL) was warmed at 45 °C for 30 minutes and then cooled. The reaction mixture was acidified with dilute AcOH. The resulting solid product was filtered and recrystallized from methanol as orange needles. Citrate-capped Au NPs were prepared according to Frens' method.[33] Briefly, 100 mL of 1 mM $HAuCl_4$ was taken into a round-bottomed flask and then boiled under vigorous stirring for 20 min. To this, 38.8 mM of trisodium citrate (10 mL) was added rapidly into the reaction flask and the mixture was stirred for another 15 min. The color of the solution changed from pale yellow to deep red, confirming the formation of Au NPs. The concentration of the Au NPs was calculated according to Beer's law by using an extinction coefficient of *ca.* 10^8 M^{-1} cm^{-1} at 520 nm (ref. 34) and found to be 12.28 nM. To obtain DTC-PAS-Au NPs, 25 μL of 1 mM DTC-PAS was added into 20 mL of Au NPs and then stirred for 1 h at room temperature (ESI,† Fig. S1). The resulting Au NP solution was used for the colorimetric sensing of Fe^{3+} in biological samples.

Detection of Fe^{3+} using DTC-PAS-Au NPs

A stock solution of ferric chloride (1 mM) was prepared by dissolving ferric chloride in deionised water. For the detection of Fe^{3+} by using the DTC-PAS-Au NPs, 100 μL of different concentrations of Fe^{3+} solution were added separately into a 1.5 mL of DTC-PAS-Au NP solution, and the pH was adjusted to 6.0 by using PBS buffer. The sample vials were vortexed for 30 s and the color of the solution changed from red to purple then blue. The resulting Au NPs UV-visible spectral changes were measured by using a Maya Pro 2000 spectrophotometer. Furthermore, we also evaluated the stability of Au NPs before and after functionalization. It was noticed that citrate modified Au NPs are stable for 2 months and well agreed with the literature.[35] At the same time, DTC-PAS-Au NPs are stable for 3–4 weeks; after that there is a slight color change due to the electrostatic interactions and hydrogen bonding formation between DTC-PAS-Au NPs. However, the rapid color change of DTC-PAS-Au NP solution (red to blue) was attributed to the DTC-PAS-Au NP aggregation induced by Fe^{3+} ion (10–100 μM).

Instrumentation

UV-visible spectra were measured with a Maya Pro 2000 spectrophotometer (Ocean Optics, USA) at room temperature. ^1H NMR spectra were recorded on a Varian 400 MHz instrument. Fourier transform infrared (FT-IR) spectra were recorded on a Perkin Elmer (FT-IR spectrum BX, Germany). Transmission electron microscopy (TEM) images were taken on a Tecnai 20 (Philips, Holland) at an acceleration voltage of 100 kV. DLS measurements were performed by using a Zetasizer Nano ZS90 (Malvern, UK).

Results and discussion

Characterization of DTC-PAS-Au NPs

The synthesized DTC-PAS-Au NPs were characterized by spectroscopic (UV-visible, FT-IR and ^{1}H NMR) and microscopic (TEM, AFM and DLS) techniques. Fig. 1 shows the UV-visible spectra of bare Au NPs and DTC-PAS-Au NPs. It can be noticed that the characteristic SPR peak (520 nm) of Au NPs was slightly red-shifted and the peak intensity was little decreased after functionalization of the DTC-PAS molecules onto the surface of the Au NPs. ESI† of Fig. S2 illustrates the typical FT-IR spectra of pure *p*-amino salicylic acid, DTC-PAS and DTC-PAS-Au NPs. FT-IR spectrum of pure *p*-amino salicylic acid shows the two characteristic bands at 3495 and 3388 cm^{-1} corresponding to –N–H asymmetric and symmetric stretching modes, respectively. The strongest absorption peak at 1644 cm^{-1} belongs to C═O stretching mode of COOH group in PAS. Fig. S2b of the ESI† shows the FT-IR spectrum of DTC-PAS. In this spectrum, C–S, –S–H and CS–NH group stretching vibrations were observed at 1100, 2561 and 1228 cm^{-1}, respectively. Importantly, it can be noticed that the mercapto group (–SH) stretching and bending modes were not observed at 2543–2550 cm^{-1} in the spectrum of the DTC-PAS-Au NPs, confirming the new bond formation between DTC-PAS and the Au NP surfaces (Fig. S2c of the ESI†). These results revealed that the DTC-PAS molecules were successfully attached onto the surface of the Au NPs *via* a simple ''zero-length'' covalent coupling.

ESI† Fig. S3 shows the ^{1}H NMR spectra of pure *p*-amino salicylic acid, DTC-PAS and DTC-PAS-Au NPs. The ^{1}H NMR spectrum of pure *p*-amino salicylic acid shows multiplet peaks at 6.0–7.0 ppm, which are assigned to the aromatic protons of PAS. The peaks at 11.37 (singlet) ppm and 12.53 (singlet) ppm corresponded to the –OH protons of PAS. The peak at 5.98 (doublet) ppm corresponds to the –NH_2 protons of PAS. The appearance of a new peak at ~1.19 ppm confirms the proton peak of the mercapto (–SH) group of DTC-PAS (ESI† Fig. S3b).

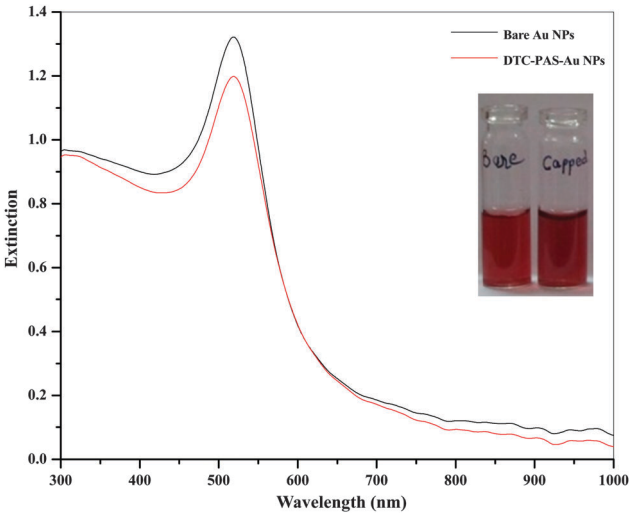

Fig. 1 UV-visible spectra of bare Au NPs (black line) and DTC-PAS-Au NPs (red line). Inset picture shows bare Au NPs and DTC-PAS-Au NPs.

However, the proton peaks of DTC-PAS-Au NPs disappeared in the spectrum of DTC-PAS-Au NPs, which confirms the change in their chemical environment and the presence of water molecules in the DTC-PAS-Au NPs (ESI† Fig. S3c).

It is well known that the average size of NPs can be estimated by calculating the mean hydrodynamic diameter from the auto-correlation function of the intensity of light scattered from the particles *via* Brownian motion.[39] Fig. 2a and b shows the DLS data of bare Au NPs and DTC-PAS-Au NPs. It is observed that the bare Au NPs are monodisperse with an average hydrodynamic diameter of ~10 nm. However, the hydrodynamic diameter of Au NPs was increased to ~43 nm due to surface modifications of Au NPs with DTC-PAS (Fig. 2b). DTC-PAS molecules are bulky and covalently attached onto the surface of the Au NPs, resulting in an increase in their hydrodynamic diameter.[40] Fig. 3a shows the TEM image of DTC-PAS-Au NPs and the functionalized Au NPs are well dispersed with an average size of ~40 nm, which agrees well with the DLS data. The DTC-PAS-Au NPs are spherical in shape. Furthermore, we also studied the AFM of DTC-PAS-Au NPs (Fig. 4a). This result indicates that the DTC-PAS-Au NPs are not aggregated and can be used as colorimetric probes for sensing of metal ions.

DTC-PAS-Au NPs as colorimetric probes for sensing Fe^{3+} ions

To investigate the analytical application of DTC-PAS-Au NPs as sensors for metal ions, various metal ions (Cu^{2+}, Fe^{2+}, Mg^{2+}, Mn^{2+}, Hg^{2+}, Zn^{2+}, Ni^{2+}, Co^{2+}, Pb^{2+}, Cd^{2+} and Fe^{3+}, 500 μM) were added into DTC-PAS-Au NP solutions (Fig. 5a). It can be observed that there is a drastic decrease in the SPR peak of DTC-PAS-Au NPs at 520 nm, and a new absorption peak is generated at 700 nm only with addition of Fe^{3+} ions, which clearly confirms the DTC-PAS-Au NP-induced aggregation with Fe^{3+} ions (Fig. 5a). This newly generated peak around 700 nm is attributed to the coordinate covalent bonds between the –OH and –COOH groups of the DTC-PAS-Au NPs and Fe^{3+}, which leads to ligand-to-metal charge transfer. As a result, the color of the DTC-PAS-Au NP solution changed from red to blue, which can be observed with the naked eye (Fig. 5b). This result strongly indicates that Fe^{3+} ions show a high ability to interact with the –OH and –COOH groups of the DTC-PAS-Au NP surfaces, resulting in DTC-PAS-Au NP-induced aggregations through electric dipole–dipole interactions and coupling between the plasmon of neighboring nanoparticles.[26] ESI† Fig. S4 shows that the colorimetric sensing ability of DTC-PAS-Au NPs with other metal species was expressed by the ratio of absorption at 700 nm to that at 520 nm ($A_{700nm/520nm}$), and indicates that DTC-PAS-Au NPs showed higher selectivity towards Fe^{3+} than the other metal species.

Sensing mechanism for Fe^{3+} ions

As shown in ESI† Fig. S1, *p*-amino salicylic acid contains amino (–NH_2), phenolic (–OH) and carboxylic acid groups (–COOH). It is well known that the –NH_2 group of PAS is already involved in the preparation of DTC-PAS followed by their molecular assembly onto the surfaces of Au NPs *via* a thiolate linkage (–NH–CS_2–Au NPs), which confirms the blocking of free –NH_2

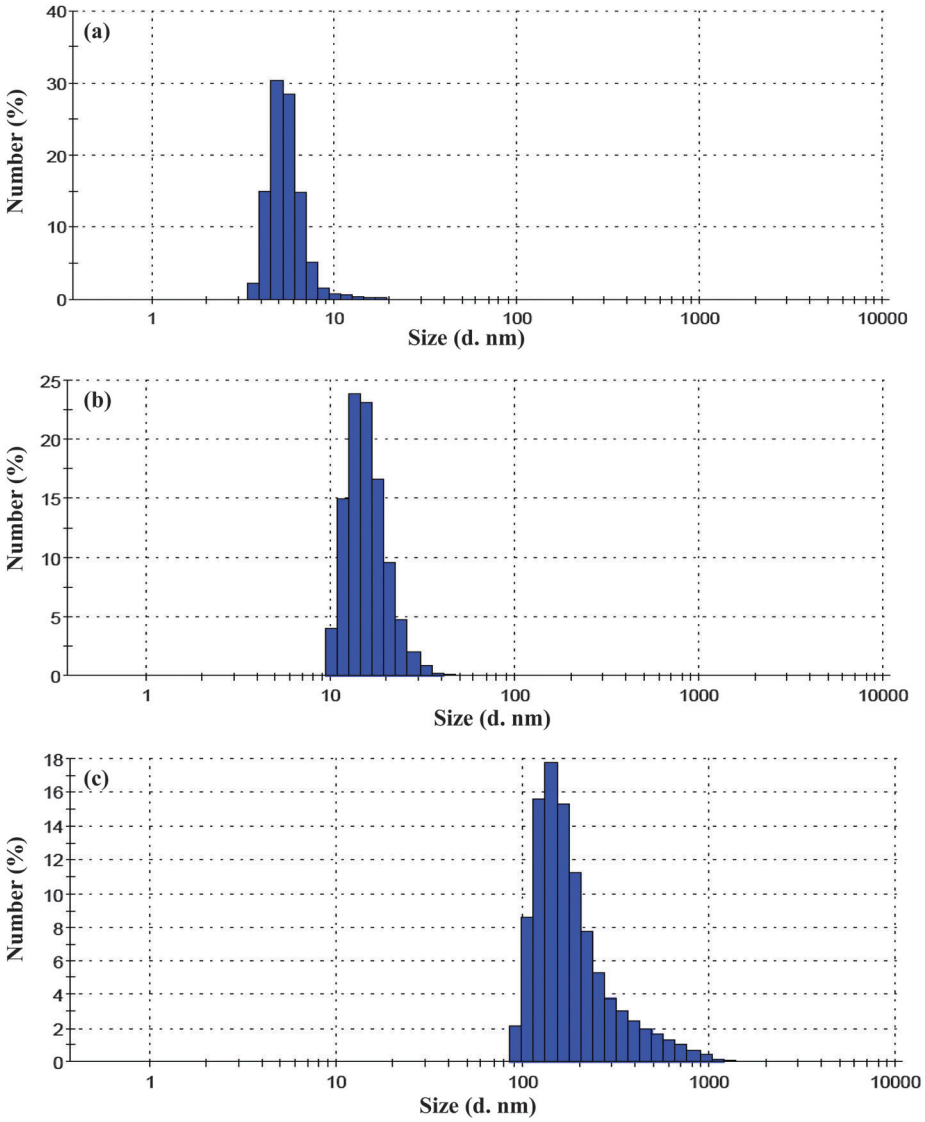

Fig. 2 DLS of (a) bare Au NPs (b) DTC-PAS-Au NPs and (c) DTC-PAS-Au NPs induced aggregations with Fe^{3+} ions.

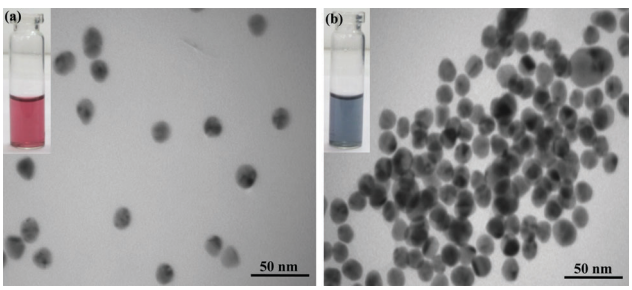

Fig. 3 TEM images of (a) DTC-PAS-Au NPs and (b) DTC-PAS-Au NPs induced aggregations with Fe^{3+} ions.

groups and avoids the complex formation of DTC-PAS-Au NPs with divalent metal ions (Fe^{2+}, Zn^{2+}, Cd^{2+}).[36] After functionalization of DTC-PAS with Au NPs, only –OH and –COOH are available to form a complex with Fe^{3+} ions. These groups have negative charges when the pH is >4. Since the pK_{a1}, and pK_{a2} values of PAS are 1.79 and 3.92 respectively, these groups are effectively coordinated with Fe^{3+} ions.[37,38] Therefore, these negatively charged groups ($-O^-$ and $-COO^-$) can be effectively form complexes with Fe^{3+}, which can induce a higher degree of DTC-PAS-Au NP aggregation.

Effect of pH

We investigated the effect of buffer pH on the colorimetric sensing ability of DTC-PAS-Au NPs for Fe^{3+} ion detection. Fig. 6 shows the intensities of the extinction ratios ($A_{700nm/520nm}$) of DTC-PAS-Au NPs upon the addition of Fe^{3+} ions in PBS, Tris and NaAc buffer systems pH from 2–10. Even though the intensities of the extinction ratios of DTC-PAS-Au NP–Fe^{3+} solutions are good when using the three buffers at low pH 2–4, this pH range is not suitable for colorimetric sensing of Au NPs. Au NPs surfaces can be neutralized at low pH (<4), which allows Au NP self aggregation without addition of analytes. As shown in Fig. 6, the extinction ratio ($A_{700nm/520nm}$) of DTC-PAS-Au NP

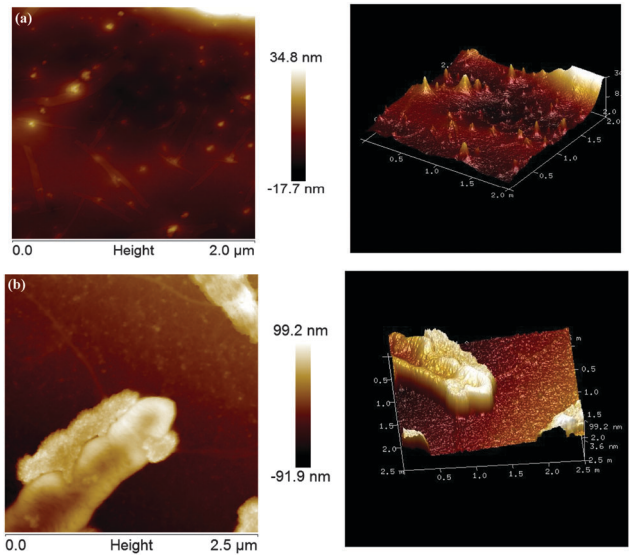

Fig. 4 AFM images of (a) DTC-PAS-Au NPs and (b) DTC-PAS-Au NPs induced aggregations with Fe^{3+} ions.

induced aggregation with Fe^{3+} ions reaches its maximum at pH 6.0. This may be because DTC-PAS-Au NPs have negative charges when the pH value is higher than 4.0, and this allows a high degree of DTC-PAS-Au NP-induced aggregation with Fe^{3+} ions. Therefore, a pH of 6.0 of the PBS buffer solution was selected.

Confirmation of DTC-PAS-Au NP-induced aggregation with Fe^{3+} ions by DLS, TEM and AFM

In order to confirm the DTC-PAS-Au NP-induced aggregation with Fe^{3+} ions, we studied DLS, TEM and AFM techniques. As shown in Fig. 2c, the hydrodynamic diameter of DTC-PAS-Au NPs was drastically increased to ~412 nm by the addition of Fe^{3+} ions, yielding the DTC-PAS-Au NP aggregation *via* the complex formation between DTC-PAS-Au NPs and Fe^{3+} ions. Fig. 3b shows the TEM image of DTC-PAS-Au NP induced aggregation with Fe^{3+} ions. It can be seen that the morphology and sizes of DTC-PAS-Au NPs were greatly influenced by the addition of Fe^{3+}, which results in a change in their state from monodisperse to polydisperse. Furthermore, the aggregation

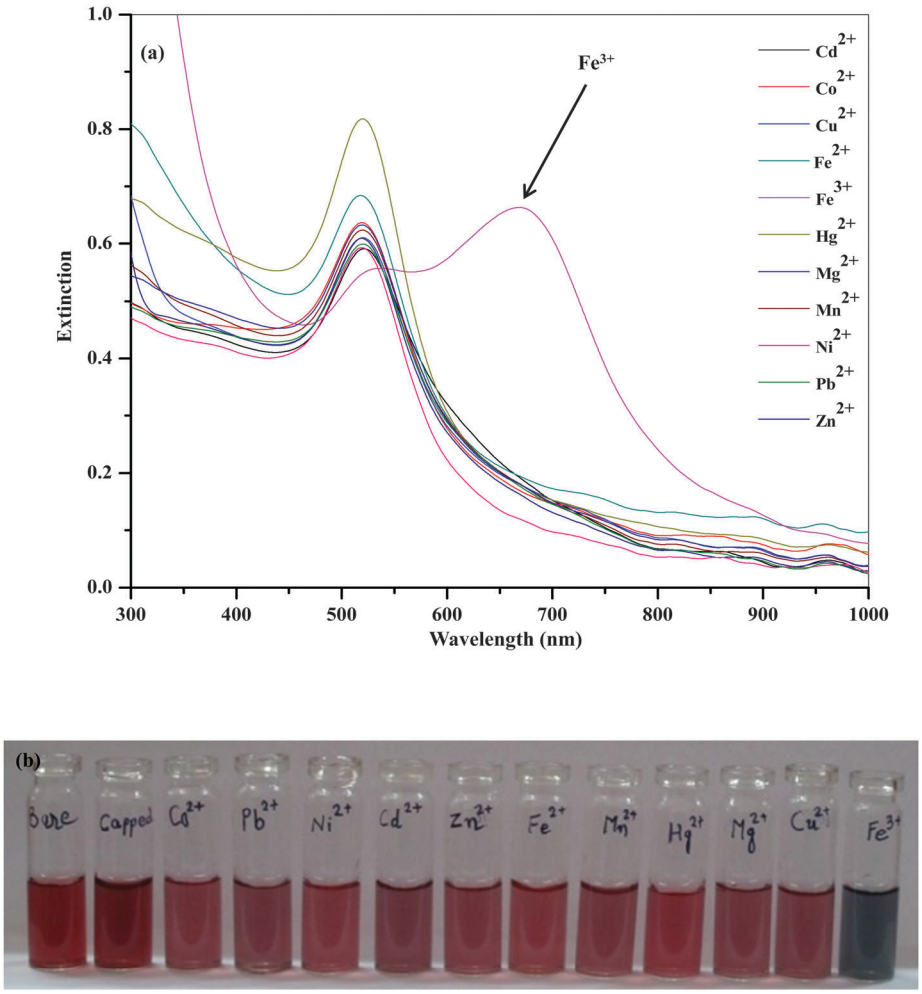

Fig. 5 (a) UV-visible absorption spectra of DTC-PAS-Au NPs upon the addition of different metal ions (Cd^{2+}, Co^{2+}, Cu^{2+}, Fe^{2+}, Fe^{3+}, Hg^{2+}, Mg^{2+}, Mn^{2+}, Ni^{2+}, Pb^{2+}, Zn^{2+}). (b) Photographic images of DTC-PAS-Au NPs in the presence of various metal ions.

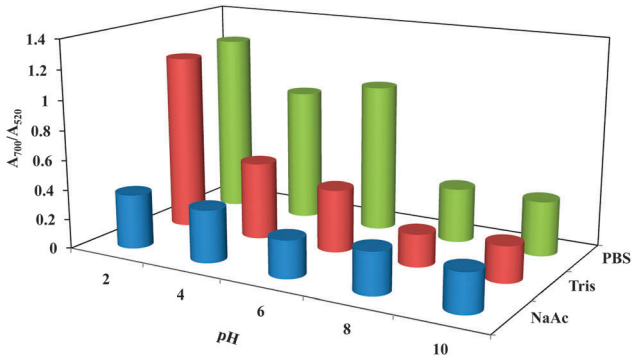

Fig. 6 The extinction ratio (A_{700nm}/A_{520nm}) of DTC-PAS-Au NP induced aggregation with Fe^{3+} ions by using different buffers (PBS, Tris and NaAc) in the pH range of 2–10.

of DTC-PAS-Au NPs with Fe^{3+} was also verified by using AFM. Fig. 4b shows the AFM image of DTC-PAS-Au NP induced aggregation with Fe^{3+} ions in three dimensions. This result confirms the DTC-PAS-Au NP induced aggregation with Fe^{3+} ions.

Quantification of Fe^{3+} by using DTC-PAS-Au NPs as colorimetric probes

The potential of the DTC-PAS-Au NP based UV-visible spectrometric method was demonstrated for the quantification of Fe^{3+} in aqueous samples as a model analytical problem. At the optimized conditions, various concentrations (10 to 100 μM) of Fe^{3+} were added into a DTC-PAS-Au NP solution separately and their UV-visible spectra were measured. As shown in Fig. 7b, the color of the Au NPs solutions gradually changed from red to purple and then blue upon increasing concentration of Fe^{3+} ions, which could be observed by the naked eye. It can be observed that with the increasing concentrations of Fe^{3+} ions, the SPR peak of Au NPs at 520 nm decreased gradually, and along with the increase a new SPR peak appeared at 700 nm (Fig. 7a). Furthermore, a calibration graph was constructed between the UV-vis extinction ratio (A_{700nm}/A_{520nm}) and concentration of Fe^{3+} ions ranging from 40 to 80 μM ($y = 1.923x - 2.846$), which can be used for the quantification of Fe^{3+} with a correlation coefficient of 0.993 (Fig. 8), and the detection limit (LOD) is 14.82 nM, respectively. In addition, we also compared the sensitivity of the present method with the reported NP-based

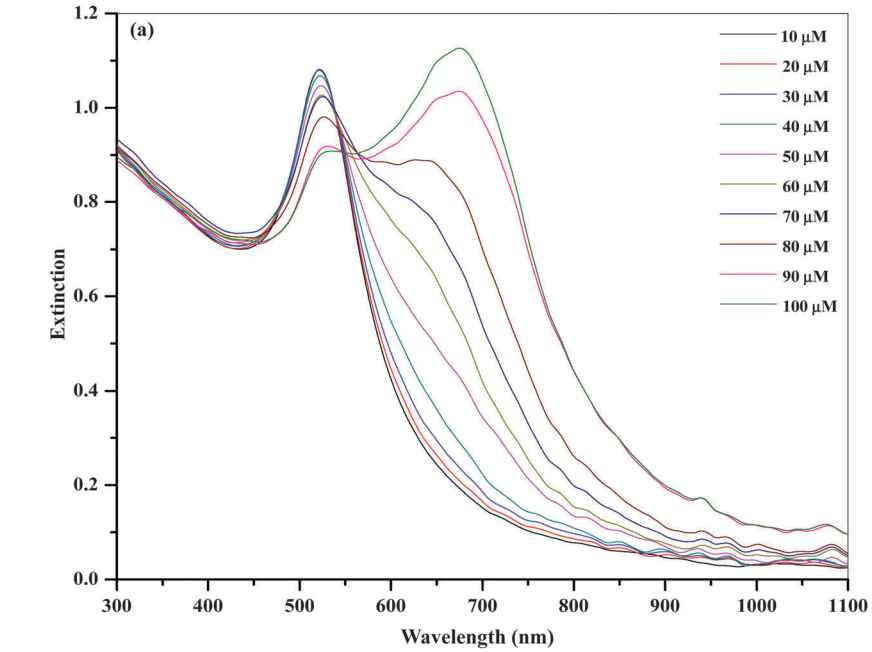

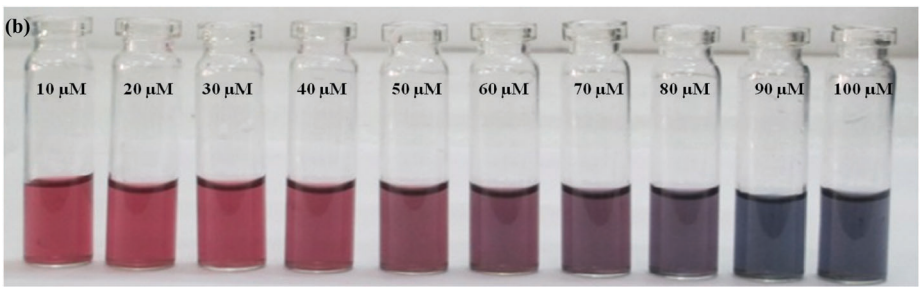

Fig. 7 (a) UV-visible spectra of DTC-PAS-Au NP solutions with increasing concentrations of Fe^{3+} in the range of 10–100 μM. (b) Visual color change of DTC-PAS-Au NPs with different concentrations of Fe^{3+} ranging from 10 μM to 100 μM.

Table 1 Comparison of DTC-PAS-Au NPs as colorimetric sensor for the detection of Fe^{3+} with the reported methods

Nanoparticles	Capping agent	Size (nm)	LOD (M)	Detection method	Ref.
Au NPs	Pyrophosphate	15	5.6×10^{-6}	UV-visible	41
Au NPs	—	—	50 ppm	UV-visible	42
Au NCs	L-3,4-Dihydroxyphenylalanine	2–6	3.5×10^{-6}	Fluorescence	43
Ag NPs	Pyridyl-appended calix[4]arene	10	125×10^{-6}	UV-visible	44
Ag NPs	p-$STEC_4$	52	9.4×10^{-9}	UV-visible	45
Carbon dots	—	3.8	0.32×10^{-6}	Fluorescence	46
Polymer dots	—	1–4	—	Fluorescence	47
Au NPs	DTC-PAS	10	14.82×10^{-9}	UV-visible	Present study

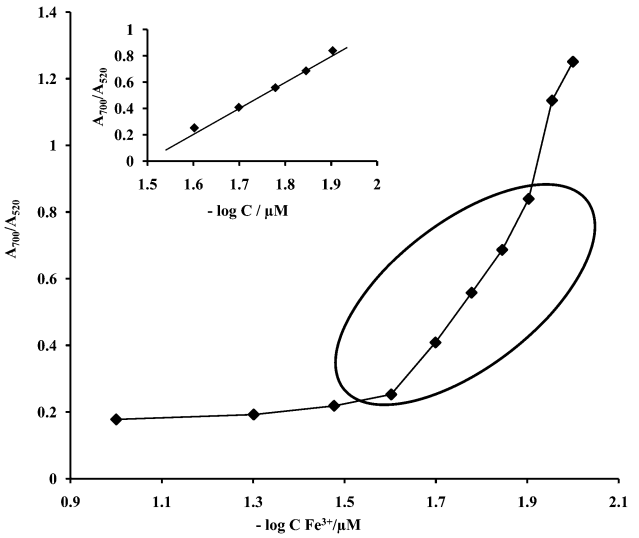

Fig. 8 Calibration graph was constructed in response to the UV-visible extinction of DTC-PAC-Au NPs solution upon the addition of Fe^{3+} ion (40–80 μM).

Table 2 DTC-PAS-Au NPs as colorimetric sensor for the analysis of Fe^{3+} in spiked blood and urine samples

Sample	Added (μM)	Found (μM)	Recovery (%)	RSD (%) (n = 3)
Blood sample	10	9.50	95.00	1.17
	50	49.03	98.06	1.18
	100	98.76	98.76	0.88
Urine sample	10	9.22	92.20	1.21
	50	47.48	94.96	1.02
	100	98.27	98.27	0.90

UV-visible and fluorescence methods for detection of Fe^{3+} ions (Table 1). It indicates that the present method showed higher sensitivity than the NPs-based UV-visible[41,42,44,45] and fluorescence[43,46,47] methods. Therefore, this analytical system exploits the advantages of DTC-PAS-Au NPs as colorimetric sensors for the detection of Fe^{3+} by using UV-visible spectrometry.

Interference studies

To demonstrate the selectivity of DTC-PAS-Au NPs for Fe^{3+} ions, competitive experiments were carried out in the presence of other metal ions (Cu^{2+}, Fe^{2+}, Mg^{2+}, Mn^{2+}, Hg^{2+}, Zn^{2+}, Ni^{2+}, Co^{2+}, Pb^{2+} and Cd^{2+}, 100 μM) for detection of Fe^{3+} ions. It can be noticed that the SPR peak shift occurred only with the mixed solution of metal ions that contained Fe^{3+} ions, resulting in a visible color change from red to blue, which was just the same as for sole addition of Fe^{3+} ions into a Au NP solution (ESI† Fig. S5). This result clearly indicates that this method was free from interference from other metal ions, which should be noted for practical application to Fe^{3+} assays in real samples.

Application of DTC-PAS-Au NPs for the analysis of Fe^{3+} ion in blood and urine samples

The proposed DTC-PAS-Au NPs sensor has been applied to detect Fe^{3+} ion in blood and urine samples. For this, human serum and urine samples were collected from healthy adult volunteers. The collected blood samples were centrifuged at 5000 rpm for 15 min. The collected supernatant (serum) were diluted 100-fold with ultrapure water and used for further analysis. Urine samples were filtered through a 0.45 μm membrane and diluted 100-fold with ultrapure water. The above blood and urine samples were spiked with different known concentrations of Fe^{3+} (10, 50 and 100 μM) and then the concentration of Fe^{3+} ions was

Table 3 Precision and accuracy of the present method for the analysis of Fe^{3+} in spiked aqueous and urine samples

		Intra-day			Inter-day		
Sample	Known concentration (μM)	Found concentration[a] (μM)	RSD[b] (%)	Accuracy[c]	Found concentration[a](μM)	RSD[b] (%)	Accuracy[c]
Spiked water	100	98.32 ± 0.0285	3.00	−0.0168	98.65 ± 0.0251	2.85	−0.0135
	50	49.08 ± 0.0115	4.35	−0.0184	50.81 ± 0.0101	4.29	+0.0162
Spiked urine	100	101.25 ± 0.044	3.95	+0.0125	97.39 ± 0.0416	3.70	−0.0261
	50	47.69 ± 0.0098	4.31	−0.0462	51.18 ± 0.0105	4.05	+0.0236

[a] Mean ± standard deviation (n = 3). [b] Relative standard deviation. [c] Accuracy was calculated from (found concentration − known concentration)/known concentration.

estimated by the aforesaid procedure. ESI† Fig. S6 shows the UV-visible spectra for the spiked blood serum and urine samples at three different concentrations (10, 50 and 100 μM). The amount of Fe^{3+} ion was estimated by using the present method and the data obtained were shown in Table 2. This result indicates that this method showed good recoveries in the range of 95–98.76% and 92.2–98.27% for blood and urine samples, with relative standard deviation (%RSD) values in the range of 0.88–1.17% and 0.90–1.21% for blood and urine samples, respectively. This indicates the present method exhibits good precision for the analysis of Fe^{3+} in blood and urine samples. In order to estimate the accuracy of the present method, we studied intra- and inter-day precision and accuracy of the method for the analysis of Fe^{3+} ion in spiked aqueous and urine samples. As shown in Table 3, this method shows good precision (RSD $<$ 4.35%) and accuracy (−0.0462 to +0.0236) for the analysis of Fe^{3+} ions in spiked aqueous urine samples. ESI† Fig. S7 shows the measured intra- and inter-day UV-visible spectra DTC-PAS-Au NPs upon the addition of Fe^{3+} ions (100 μM). These results indicate the reliability of DTC-PAS-Au NPs as ideal colorimetric probes for Fe^{3+} determination in real samples.

Conclusions

In summary, we present a simple, selective and sensitive DTC-PAS-Au NP-based UV-visible method for on-site and real-time detection of Fe^{3+} in biological samples. The Fe^{3+} ion-induced aggregates of DTC-PAS-Au NPs were characterized by UV-visible spectroscopy, DLS, TEM and AFM, respectively. The extinction ratio A_{700nm}/A_{520nm} is linear with the concentration of Fe^{3+} ranging from 40 μM to 80 μM, which provides a sensitive detection of Fe^{3+} ions with a detection limit of 14.82 nM. This method was free from interference from other metal ions and exhibited good precision and accuracy for detection of Fe^{3+} ions in aqueous and urine samples. Therefore, DTC-PAS-Au NPs can be utilized as a novel colorimetric sensor for the rapid, selective and real-time *in situ* detection of Fe^{3+} in biological samples, and it offers great potential for practical applications to Fe^{3+} ion assays in environmental and biological samples.

Acknowledgements

We gratefully acknowledge the Director, SVNIT for providing all the facilities to carry out this work. We also thank the Department of Science and Technology, India for providing a UV-visible spectrophotometer for this analysis. We would like to thank Mr Vikas Patel, SICART, Anand, and V. V. Nagar for their assistance in TEM data. The authors thank Shivam Pathological Laboratory, Surat, Gujarat, India for providing blood samples.

References

1 A. P. de Silva, H. Q. N. Gunaratne, T. Gunnlaugsson, A. J. M. Huxley, C. P. Mccoy, J. T. Rademacher and T. E. Rice, *Chem. Rev.*, 1997, **97**, 1515.
2 K. Rurack and U. R. Genger, *Chem. Soc. Rev.*, 2002, **31**, 116.
3 V. Amendola, L. Fabbrizzi, F. Forti, M. Licchelli, C. Mangano, P. Pallavicini, A. Poggi, D. Sacchi and A. Taglieti, *Coord. Chem. Rev.*, 2006, **250**, 273.
4 D. T. Quang and J. S. Kim, *Chem. Rev.*, 2010, **110**, 6280.
5 R. H. Holm, P. Kennepohl and E. I. Solomon, *Chem. Rev.*, 1996, **96**, 2239.
6 R. Meneghini, *Free Radical Biol. Med.*, 1997, **23**, 783.
7 R. S. Eisenstein, *Annu. Rev. Nutr.*, 2000, **20**, 627.
8 T. A. Rouault, *Nat. Chem. Biol.*, 2006, **2**, 406.
9 J. A. Cowan, *Inorganic Biochemistry: An Introduction*, Wiley-VCH, New York, 1997, p. 167.
10 C. Brugnara, *Clin. Chem.*, 2003, **49**, 1573.
11 J. D. Haas and T. Brownlie IV, *J. Nutr.*, 2001, **131**, 676.
12 O. K. Fix and K. V. Kowdley, *Minerva Med.*, 2008, **99**, 605.
13 P. Aisen, M. W. Resnick and E. A. Leibold, *Curr. Opin. Chem. Biol.*, 1999, **3**, 200.
14 K. Pomazal, C. Prohaska, I. Steffan, G. Reich and J. F. K. Huber, *Analyst*, 1999, **124**, 657.
15 M. E. C. Busto, M. M. Bayon, E. B. Gonzalez, J. Meija and A. S. Medel, *Anal. Chem.*, 2005, **77**, 5615.
16 G. L. Arnold, S. Weyer and A. D. Anbar, *Anal. Chem.*, 2004, **76**, 322.
17 J. E. T. Andersen, *Analyst*, 2005, **130**, 385.
18 C. M. G. van den Berg, *Anal. Chem.*, 2006, **78**, 156.
19 D. C. Hone, A. H. Haines and D. A. Russell, *Langmuir*, 2003, **19**, 7141.
20 S. H. Wu, Y. S. Wu and C. H. Chen, *Anal. Chem.*, 2008, **80**, 6560.
21 J. S. Lee, M. S. Han and C. A. Mirkin, *Angew. Chem., Int. Ed.*, 2007, **46**, 4093.
22 D. Li, A. Wieckowska and I. Willner, *Angew. Chem., Int. Ed.*, 2008, **47**, 3927.
23 S. Kubo, A. Diaz, Y. Tang, T. S. Mayer, I. C. Khoo and T. E. Mallouk, *Nano Lett.*, 2007, **7**, 3418.
24 M. C. Daniel and D. Astruc, *Chem. Rev.*, 2004, **104**, 293.
25 H. Li, Q. Zheng and C. Han, *Analyst*, 2010, **135**, 1360.
26 H. Cao, M. Wei, Z. Chen and Y. Huang, *Analyst*, 2013, **138**, 2420.
27 P. Morf, F. Raimondi, H. G. Nothofer, B. Schnyder, A. Yasuda, J. M. Wessels and T. A. Jung, *Langmuir*, 2006, **22**, 658.
28 S. K. Kailasa and H. F. Wu, *Analyst*, 2012, **137**, 1629.
29 A. Pandya, K. V. Joshi, N. R. Modi and S. K. Menon, *Sens. Actuators, B*, 2012, **168**, 54.
30 V. N. Mehta, A. K. Mungara and S. K. Kailasa, *Anal. Methods*, 2013, **5**, 1818.
31 V. N. Mehta, A. K. Mungara and S. K. Kailasa, *Ind. Eng. Chem. Res.*, 2013, **52**, 4414.
32 M. S. I. T. Makki, R. M. Abdel-Rahman, H. M. Faidallah and K. A. Khan, *J. Chem.*, 2013, 862463, DOI: 10.1155/2013/862463.
33 G. Frens, *Nat. Phys. Sci.*, 1973, 20.
34 C. C. Huang and H. T. Chang, *Chem. Commun.*, 2007, 1215.
35 S. H. Brewer, W. R. Glomm, M. C. Johnson, M. K. Knag and S. Franzen, *Langmuir*, 2005, **21**, 9303.
36 L. Qi, Y. Shang and F. Wu, *Microchim. Acta*, 2012, **178**, 221.

37 W. A. E. McBryde, J. L. Rohr, J. S. Penciner and J. A. Page, *Can. J. Chem.*, 1970, **48**, 2574.
38 X. X. Ou, X. Quan, S. Chen, F. J. Zhang and Y. Z. Zhao, *J. Photochem. Photobiol., A*, 2008, **197**, 382.
39 X. Liu, Q. Dai, L. Austin, J. Coutts, G. Knowles, J. Zou, H. Chen and Q. Huo, *J. Am. Chem. Soc.*, 2008, **130**, 2780.
40 Q. Wang, L. Yang, X. Yang, K. Wang and J. Liu, *Analyst*, 2013, **138**, 5146.
41 S. P. Wu, Y. P. Chen and Y. M. Sung, *Analyst*, 2011, **136**, 1887.
42 S. K. Tripathy, J. Y. Woo and C. S. Han, *Sens. Actuators, B*, 2013, **181**, 114.
43 J. A. Ho, H. C. Chang and W. T. Su, *Anal. Chem.*, 2012, **84**, 3246.
44 J. Zhan, L. Wen, F. Miao, D. Tian, X. Zhu and H. Li, *New J. Chem.*, 2012, **36**, 656.
45 A. Pandya, P. G. Sutariya, A. Lodha and S. K. Menon, *Nanoscale*, 2013, **5**, 2364.
46 K. Qu, J. Wang, J. Ren and X. Qu, *Chem.–Eur. J.*, 2013, **19**, 7243.
47 T. Lai, E. Zheng, L. Chen, X. Wang, L. Kong, C. You, Y. Ruan and X. Weng, *Nanoscale*, 2013, **5**, 8015.